Paleoseismicity and seismic hazard in southern Patagonia (Argentina-Chile; 50°–55°S) and the role of the Magallanes-Fagnano transform fault

Gustavo González Bonorino, Víctor Rinaldi, Liliana del Valle Abascal, Patricia Alvarado, Gustavo G. Bujalesky & Arturo Güell

Natural Hazards
Journal of the International Society for the Prevention and Mitigation of Natural Hazards

ISSN 0921-030X

Nat Hazards
DOI 10.1007/s11069-011-9917-2

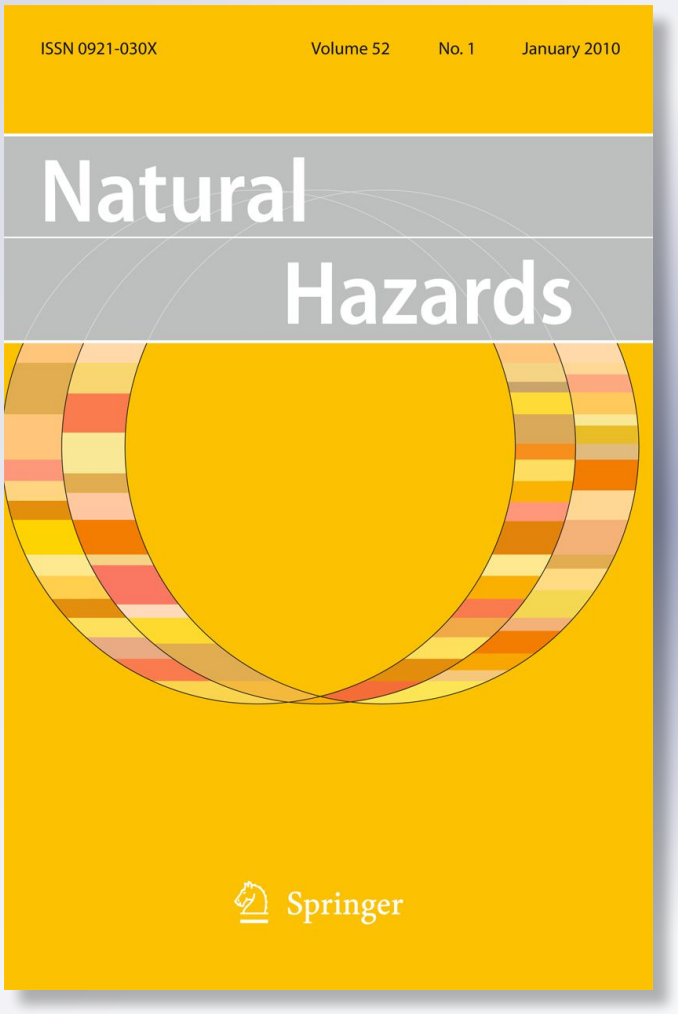

Springer

Nat Hazards
DOI 10.1007/s11069-011-9917-2

ORIGINAL PAPER

Paleoseismicity and seismic hazard in southern Patagonia (Argentina-Chile; 50°–55°S) and the role of the Magallanes-Fagnano transform fault

Gustavo González Bonorino · Víctor Rinaldi · Liliana del Valle Abascal · Patricia Alvarado · Gustavo G. Bujalesky · Arturo Güell

Received: 21 July 2010 / Accepted: 25 July 2011

Abstract Patagonia, including the island of Tierra del Fuego, lies in southernmost South America at the junction of the South American, Antarctic, and Scotia tectonic plates. Historical and instrumental records have documented several local earthquakes of damaging magnitude, posing a threat to the rapidly growing population of 300,000 and the expanding industrial and service infrastructure. Short and inaccurate instrumental records of local seismic events and a diffuse epicenter distribution not clearly related to the recognized seismogenic structures have hindered an adequate evaluation of the seismic hazard for this region. To improve this situation, a paleoseismological study was carried out on two gravelly strandplains on the Atlantic coast of Patagonia. Surveying combined ground-probing radar, vertical electric sounding, and seismic refraction. Coseismic normal faults buried beneath the strandplain bodies were revealed and related to the morphology of the strandplains. The faults have probable ages between 0.9 and 6.4 kyr BP and a recurrence rate of about 1 kyr. The more likely source for these structures is the Magallanes-Fagnano fault, a continental transform fault that crosses Tierra del Fuego. The distance of more than 300 km from the buried coseismic structures to the trace of the Magallanes-Fagnano fault argues for high-magnitude earthquake activity on this fault throughout the Holocene. Urban development on soft glacial and alluvial substrates increases the hazard.

G. G. Bonorino (✉) · G. G. Bujalesky
CONICET-CADIC, B Houssay 200, CP9410 Ushuaia, Argentina
e-mail: g_bonorino@yahoo.com.ar

V. Rinaldi
Facultad de Ciencias Exactas, Universidad Nacional de Córdoba, Av. Vélez Sarsfield 1601, CP5000 Córdoba, Argentina

L. del Valle Abascal
UTN-FRRG, Islas Malvinas 1650, CP9420 Rio Grande, Argentina

P. Alvarado · A. Güell
CONICET-Departamento de Geofisica y Astronomía, Universidad Nacional de San Juan, Meglioli 1160, CP5406 San Juan, Argentina

Published online: 12 August 2011

Keywords Paleoseismology · Seismic hazard · Tierra del Fuego · South America · Coseismic deformation

1 Introduction

Patagonia designates territory in southernmost South America shared by Argentina and Chile (Fig. 1, inset). The region of interest to this paper lies in southern Patagonia, comprising the island of Tierra del Fuego and neighboring lands north of the Strait of Magellan (Fig. 1). The population of about 300,000 is concentrated in six rapidly growing urban areas: Río Gallegos, Río Grande, Tolhuin and Ushuaia, in Argentina, and Porvenir and Punta Arenas, in Chile (Fig. 1). Hydrocarbon extraction is a major activity on both the Atlantic and the Pacific seaboards of Patagonia, and oil and gas pipelines have been laid across the region; industrial and lifeline infrastructure is likewise rapidly expanding. Southern Patagonia lies in a region of frequent and intense seismic activity, and significant seismogenic structures have been recognized both onshore and offshore, at the junctions between the South American, Antarctic, and Scotia tectonic plates (Fig. 1, inset). The instrumental record of seismic local events in Patagonia spans less than a decade, and historical seismicity accounts date back no further than the late nineteenth century (http://www.inpres.gov.ar). Nonetheless, they suffice to ascertain the occurrence of local seismic events of large magnitude ($M \geq 7$) with epicenters in southern Patagonia and the neighboring offshore zone. In 1879, Rev. Thomas Bridges, an Anglican missionary settled in Ushuaia, witnessed an earthquake that spilled liquids from containers and hindered walking. Based on an isoseismal analysis, Martinic (2008) estimated a maximum Mercalli intensity of VIII for this event, and set the epicenter a short distance south of Punta Arenas. In more modern times, two $M = 7.8$ earthquakes took place in 1949, when the population

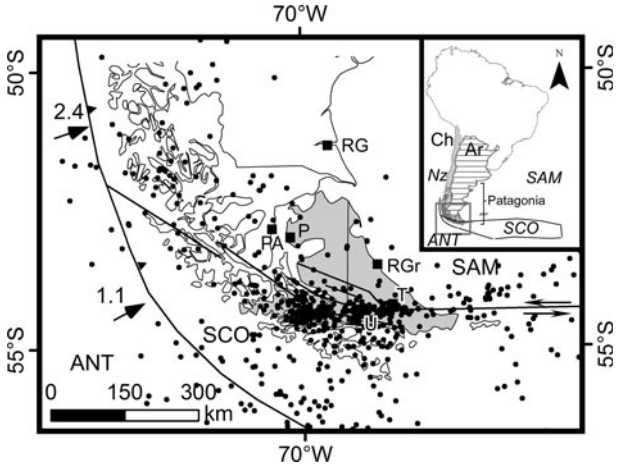

Fig. 1 Seismotectonic setting of southern Patagonia. The *inset* shows the plate tectonic setting of Patagonia; the small rectangle encompasses the study area. *Ch* Chile, *Ar* Argentina, tectonic plates—*Nz* Nazca, *SAM* South American plate, *SCO* Scotia plate, *ANT* Antarctic plate. Main panel—*dots* are epicenters from Febrer et al. (2001). Localities—*RG* Río Gallegos, *RGr* Río Grande, *U* Ushuaia, *PA* Punta Arenas, *P* Porvenir. *Arrows* with decimal numbers on left side indicate convergence velocity of Antarctic plate in cm/year, from Pelayo and Wiens (1989) and DeMets et al. (1990). Tierra del Fuego island is shown in *gray*. *Solid lines* are faults

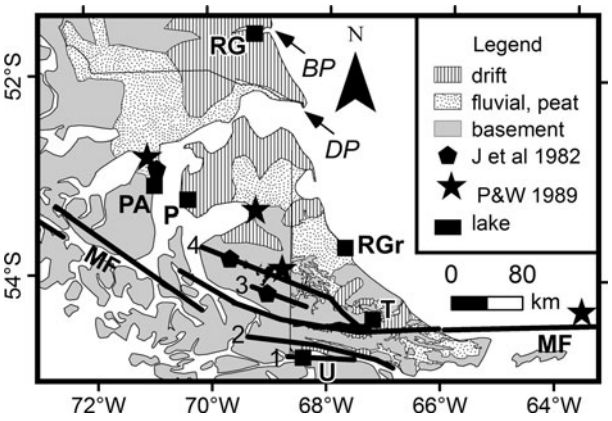

Fig. 2 Simplified geologic map of southern Patagonia, with emphasis on the Quaternary (data mainly from SERNAGEOMIN 2003; SEGEMAR 2004). Localities (*squares*)—*RG* Río Gallegos, *RGr* Río Grande, *U* Ushuaia, PA *Punta Arenas*, *P* Porvenir. Strike-slip faults: *1* Beagle Channel, *2* Larsifashaj, *3* Deseado, *4* unnamed, and *MF* Magallanes-Fagnano. Study areas: *BP* Bustamante Point, *DP* Dungeness Point. *P&W 1989* epicenters for the 1949, 1950, and 1970 earthquakes (*stars*) from Pelayo and Wiens (1989); *J et al. 1982* epicenters for the 1949 and 1950 events (*pentagons*) from Jaschek et al. (1982)

in southern Patagonia was one-twentieth of that at present, and industrial and lifeline infrastructure was virtually non-existent. Thus, despite the high energy released by these crustal earthquakes, only moderate damage and minor human casualties were observed. At present, a similar magnitude earthquake could result in severe consequences if an adequate earthquake hazard evaluation is not considered in engineering designs.

In view of the shortage of information on the seismic nature of southern Patagonia, paleoseismology is an appealing resource for improving the estimate of the local seismic hazard (Abascal and González-Bonorino 2008). This paper gives evidence for coseismic faulting in southern Patagonia and relates it to seismic hazard in the island of Tierra del Fuego. Exploration for coseismic structures centers on two strandplains on the Atlantic coast north of the Strait of Magellan: Bustamante Point and Dungeness Point (Fig. 2). Multiple geophysical techniques, ground-probing radar, vertical electric sounding, and seismic refraction, are combined to visualize coseismic structures buried beneath the strandplain gravel. The potential sources for the deformation are then analyzed and ranked in terms of seismic hazard for Tierra del Fuego, taking into account potential site effects. Vertical coseismic displacement of littoral deposits over wide coastal expanses has been documented previously (e.g., Ramírez-Herrera et al. 2004). In contrast, this paper identifies local, specific causative coseismic structures.

2 Geologic and seismotectonic setting

The core of the Andes in southern Patagonia consists of Jurassic and Cretaceous igneous and metamorphic rocks flanking the Pacific Ocean. Eastward and northeastward from this core extend Tertiary marine and continental sandstone and shale that underlie the Andean fold and thrust belt. Quaternary glacigenic deposits (basal till, periglacial moraines, and glacio-lacustrine deposits), herein collectively designated drift, mantle the foreland strata, and floodplain sediments and peat bogs occupy fluvial and glacial valleys throughout the

region. Basal till and moraine deposits form compacted bodies up to 40 m in thickness resting on bedrock. Till yields penetration resistance (Standard Penetration Test, SPT) values $N = 20$ to refusal and classifies as NEHRP Site Class D, "stiff soil." Gravel-rich alluvium several meters thick is tentatively classified as NEHRP Site Class D, "stiff soil." Thick (ca 20 m thick) glacio-lacustrine deposits in suburban Tolhuin, and peat bogs several meters in thickness at various localities, classify as NEHRP Site Class F, "soils requiring geotechnical analysis." All the urban centers mentioned above occupy, partly or entirely, areas of soft and firm soil (Fig. 2).

In southern Patagonia, the structural strike of the Andes changes from a north–south to an east–west orientation. The pronounced curvature is related to Oligocene–Miocene pervasive east–west shear and formation of the North Scotia ridge, a left-lateral transform fault separating the South American and the Antarctic plates, and cutting across the island of Tierra del Fuego (Fig. 1; Pelayo and Wiens 1989; Klepeis 1994). The continental segment of this transform fault is known as the Magallanes-Fagnano (MF) fault (Klepeis 1994; Lodolo et al. 2003). The principal trace of the MF fault is, in fact, a series of vertical fault segments arranged with an *en échelon* geometry and shows a restraining bend between 68°30'W and 70°W, with a northward concavity (Fig. 1; Smalley et al. 2003; Lodolo et al. 2003). Geodetic GPS measurements indicate relative motion across the MF fault system at rates between 0.66 and 0.96 cm/year (Smalley et al. 2003; DeMets et al. 2010). The MF fault is one of the set of subparallel strike-slip faults including, from south to north, the Beagle Channel, Larsifashaj, MF, Deseado, and other faults (Fig. 2; Klepeis 1994; Menichetti et al. 2008). Velasco et al. (2002) speculated that the site of active strike-slip faulting migrated northward, thus leaving the Beagle Channel and Larsifashaj faults as inactive and concentrating present tectonic activity on the main MF fault and subsidiary faults to the north.

West and southwest of Tierra del Fuego, the Antarctic plate subducts beneath the South American plate at a rate of 2.4 cm/year (DeMets et al. 1990) and beneath the Scotia plate at a slower rate of 1.1 cm/year (Pelayo and Wiens 1989). This segment of the Chile subduction zone appears to generate only weak seismic events, probably due to the slow velocity of convergence and the diffuse Benioff zone (Barrientos 2007).

The crustal structure beneath southern Patagonia is not well known. Project SEPA (Seismic Experiment in Patagonia and Antarctica; 1997–1998; Lawrence and Wiens 2004) identified the Moho at a depth of 32 km beneath central Tierra del Fuego. Beneath the continental shelf southwest of Tierra del Fuego, the Moho lies at a shallower depth of about 25 km (Rubio et al. 2000). The crustal thickness in this region is less than the global average of 41 km for continental regions (Christensen and Mooney 1995). Smalley et al. (2003) postulated that the down-dip end of the main MF fault probably lies at a depth of approximately 15 km, that is, within the crust. Shallow focal depths increase the seismic hazard in the region of study.

3 Historical earthquake locations

Seismic station USHU, near the city of Ushuaia, part of the Antarctic Seismographic Argentinean Italian Network (ASAIN), and stations abroad have recorded a persistent small- to moderate-magnitude ($M < 6$) seismic activity (Febrer et al. 2001; NEIC catalogue). Very few epicenters fall in the neighborhood of Río Gallegos and in northern Tierra del Fuego, suggesting an absence of seismogenic sources in that region. A large number of the epicenters lie above the Antarctic–South American subduction zone and near the MF

fault, but many do not show a clear association with these structures (Fig. 1). The lack of a local seismic network but also the weakness of the corresponding seismic arrivals hinder accurate epicenter location. The short historical and instrumental record of seismic activity in southern Patagonia includes several significant events that should provide firmer data on epicenter location. Instrumental records show four high-magnitude earthquakes with epicenters on Tierra del Fuego. Two of these events occurred on December 17, 1949, at 06:53:30 GMT, the foreshock and at 15:07:55 GMT, the mainshock, both with estimated magnitudes of $M = 7.8$. These events rank third in magnitude among earthquakes recorded in southern South America, after the 1960 $M = 9.5$ Valdivia and the 2010 $M = 8.8$ Maule earthquakes in Chile. A strong aftershock with $M = 7.0$ took place on January 30, 1950. A further seismic event ($M = 7.0$) took place on June 15, 1970. Pelayo and Wiens (1989) set the epicenters for the two stronger events at a considerable distance from the MF fault (Fig. 2). According to Adaros et al. (1999), "the fault along which the 1949 $M = 7.8$ earthquakes occurred has never been firmly established".

Jaschek et al. (1982) used additional regional seismic data to relocate the 1949 earthquake epicenters closer to the MF fault zone. Triangulation and data from seismological stations BAA (Buenos Aires, Argentina), SAN (Santiago, Chile), and LPZ (La Paz, Bolivia) indicate that epicenter locations in Jaschek et al. (1982) are more consistent with regional and global data than those in Forsythe (1975) and in Pelayo and Wiens (1989).

The felt area of the higher-magnitude earthquakes, such as the 1879 and 1949 events, extended as far north as 50°S, north of Rio Gallegos (Martinic 2008; Costa et al. 2006), warranting a search for evidence of Holocene coseismic deformation in continental Argentina, north of Tierra del Fuego island.

4 Coseismic deformation in strandplains

Holocene strandplains in southern Patagonia started to develop when the rate of postglacial sea level rise waned, about 7 kyr ago, equaling and then falling slightly below the rate of tectonic uplift driven by Andean orogenesis (Milne et al. 2005). Strandplains yield extensive tabular bodies of laterally accreting, gravelly shoreline deposits resting on wave-cut surfaces. The subaerial surfaces of the strandplains expose berm and backbeach sediments organized in rectilinear to gently curved ridges and swales. The three-dimensional arrangement of the ridges is fundamentally controlled by storm wave run-up height and direction, which, in turn, are modulated by nearshore bathymetry. Uplift or subsidence of a wave-cut surface relative to sea level will be reflected in the organization of the strandplain ridges.

The tabular geometry and growth protracted in time make strandplains good targets for the geologic records of coseismic faulting. It may, however, prove difficult from the study of strandplain morphology alone to document coseismic fault offsets hidden beneath the strandplain body. Geophysical techniques provide tools for independent recognition of coseismic deformation affecting the strandplain body. This study combined vertical electric sounding, seismic refraction, and ground-probing radar techniques to explore for coseismic structures.

4.1 Strandplain morphology and age

The Bustamante and Dungeness strandplains rest on horizontal Tertiary strata through wave-cut erosion surfaces that are exposed during neap tides (tidal range is 8 m) at about

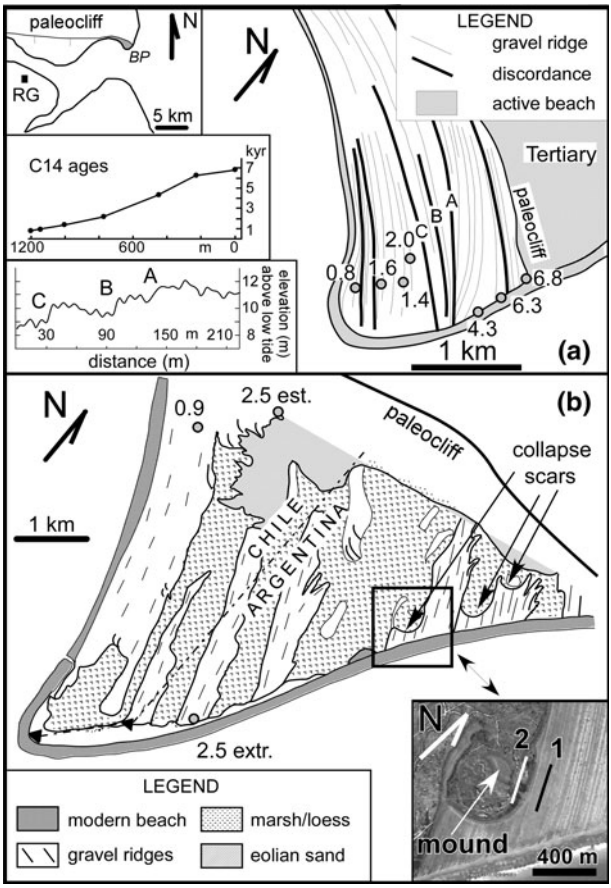

Fig. 3 **a** Morphologic map of Bustamante Point. Gravel ridges are shown schematically by *thin lines* and discordances by *thick lines*; three discordances are designated *A*, *B*, and *C*. *Circles* and *numbers* indicate sample site and age in kiloyears. *Uppermost inset* on the left shows position of Bustamante Point at the mouth of the Gallegos River estuary. The *central inset* is a plot of radiometric ages versus distance from the paleocliff. *Lowermost inset* shows a topographic profile of gravel ridges showing steps in the strandplain. **b** Morphologic map of Dungeness Point (modified after Uribe and Zamora 1981 and González Bonorino et al. 1999). *Circles* and *numbers* indicate sample site and age in kiloyears; age 2.5 est. was estimated by Uribe and Zamora (1981); age 2.5 extr. is an extrapolation in this paper. *Inset* in the bottom right corner shows an aerial photograph of the surveyed collapse structure with locations of the seismic refraction and VES transects on the high strandplain (*1*) and within the collapse structure (*2*). A gravel mound rises within the collapsed area and a small spit bar occurs on its seaward side

12–13 m below the top of the strandplains (González Bonorino et al. 1999). Both strandplains are attached to paleocliffs carved in Quaternary glacial drift and Tertiary shallow marine deposits and show a consistent drop in average elevation by about 3–4 m, in the younging direction, reflecting a fall in relative sea level attributed to Andean tectonics (Bujalesky 2007).

The Bustamante strandplain measures 4.5 km along its landward edge and projects 1.5 km into the Gallegos River estuary (Fig. 3a, uppermost inset). The Atlantic flank of the strandplain is under erosion and exposes the upper 3 m of the gravel body, with seaward-dipping foreshore beds. Surficially, the strandplain shows a series of gravel ridges with

mean amplitude of 0.26 cm (crest to trough) organized in about half-dozen bundles separated by discordances, or abrupt changes in average crest trend in plan view. These discordances reflect major hydraulic reorganizations. In most cases, discordances are associated with marked drops in elevation of the gravel platform by 0.5–0.7 m, that is, more than twice the average ridge amplitude, with the younger ridges on the downthrown side (Fig. 3a, lowermost inset). Radiocarbon ages were obtained from fossil shelly fauna (*Mytilus* sp.; mussel) buried in the strandplain gravel. The reservoir effect was partially compensated for by analyzing the carbon content in living *Mytilus* sp. The ages indicate that growth of the platform started at about 7 kyr BP and progressed to the present with an approximately linear trend (Fig. 3a, central inset; E. Linares 1996; written communication).

Dungeness Point (so named by eighteenth century sailors to acknowledge morphological similarities with Dungeness Spit in England) measures 8 km along the landward side and projects 7 km into the Strait of Magellan (Fig. 3b). The strandplain shows bundles of gravel ridges separated by intercalations of marsh deposits (Fig. 3b; Uribe and Zamora 1981). Semicircular scars dissect several of the older gravel bundles (Fig. 3b, inset; González Bonorino et al. 1999). Across each scar, the ground falls abruptly by several meters and then rises into a central mound whose summit lies below the top of the strandplain. The low ground between the high strandplain and the mound is filled with marsh deposits; the mound crest consists of gravel finer than that in the ridge crests in the strandplain. From the Chilean sector of Dungeness Point, Uribe and Zamora (1981) reported a radiocarbon age of 0.9 kyr BP on cetacean remains and estimated an age of 2.5 kyr BP for the oldest beach ridges (Fig. 3b). Herein, this age was visually extrapolated to the Argentine sector (Fig. 3b).

4.2 Geophysical surveys

Geophysical work was carried out at two sites: (a) a prominent discordance (discordance A in Fig. 3a) and associated drop in strandplain elevation at Bustamante Point and (b) a collapse structure at Dungeness Point (Fig. 3b). Shallow seismic refraction was performed using a 12-geophone line connected to a Geometrics seismograph. Seismic energy was generated by the impact of a 7-kilogram hammer. The low energy applied limited the length of the line deployment to 50 m and, accordingly, the investigation depth. No explosives were allowed due to environmental concerns. Data interpretation was performed following the simple reciprocal method (Palmer 1980). The vertical electrical soundings (VES) were performed by the means of a 300 W MP Argentine resistivity meter. Current electrodes (AB) were opened up to a maximum of one hundred meters. The Schlumberger configuration was used in conjunction with specific software for electrical data interpretation. A detailed description of the method can be found elsewhere (e.g., Sharma 1986; US Army Corps of Engineers 1995). Finally, the subsurface interface radar system SIR2000, manufactured by Geophysical Survey System Inc (GSSI) was used with a shielded antenna having a central frequency of 200 MHz. Procedures for the design of the GPR survey and data processing can be found in Annan (1992).

On the Bustamante strandplain, seismic refraction revealed four velocity layers: (1) a 1-m-thick upper layer with compressional seismic wave velocities of 200 m/s, (2) a 6-m-thick layer yielding a velocity of 420 m/s, (3) a 5-m-thick layer with velocity of 1,500 m/s, and (4) a bottom layer with velocity of 2,100 m/s (Fig. 4a, upper left-hand side). Exposures of the strandplain along the Atlantic shoreline and GPR surveys (see below) support associating the upper two layers with berm and foreshore gravel and sand with very low

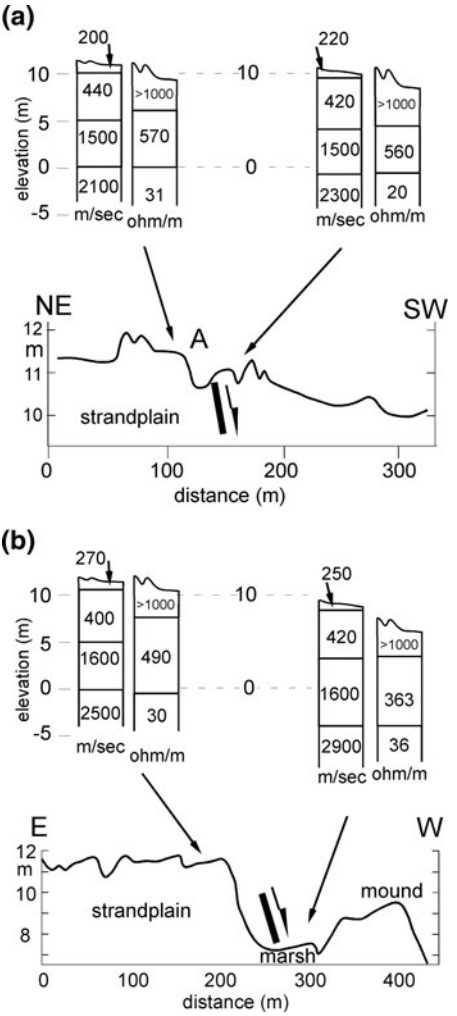

Fig. 4 **a** Refraction seismic and geoelectric profiles on Bustamante Point at either side of discordance *A* (see location in Figs. 2, 3). Interpreted topographic section shows a normal fault. **b** Refraction seismic and geoelectric profiles on Dungeness Point at either side of the scarp bounding the collapse structure (see location in Figs. 2, 3). Interpreted topographic section shows a normal fault. Geophysical sections are referred to the top of the Tertiary exposed at neap low tide. The *dashed lines* are drawn for reference

moisture content. The layer with seismic velocity of 1,500 m/s is interpreted to lodge the water table in lower foreshore and beach toe sand. The bottom layer with top at 0 m and highest velocity would correlate with the Tertiary bedrock exposed at neap low tide. The vertical electrical sounding distinguished three layers: (1) an upper layer of very high electrical resistivity in excess of 1,000 Ω-m, (2) a central 5-m-thick layer with an electrical resistivity of 550 Ω-m, and (3) a low resistivity substrate (Fig. 4a, upper right-hand side). The uppermost layer largely correlates with the upper two layers in the seismic profile, but its base occurs about 2 m higher than the base of the second seismic layer; this is attributed to capillary rise of water from the water table reducing the resistivity. The bottom layer with very low electrical resistivity and top at 0 m correlates with the argillaceous Tertiary bedrock. The seismic refraction and VES profiles on the downthrown side show a similar stratigraphy, displaced downward about 1 m. The geophysical surveys on the strandplain at Dungeness Point revealed a geophysical stratigraphy identical to that at Bustamante Point

and are similarly interpreted (Fig. 4b). On the downthrown side, the seismic refraction and VES profiles suggest downward displacement by about 4 m.

The GPR surveys transverse to ridge crests at Bustamante Point and at Dungeness Point away from the circular collapse structure show the typical rhythmic foreset architecture of foreshore facies. At Dungeness Point, two perpendicular GPR profiles were surveyed across the gravel mound within the collapse structure to determine if the mound is a displaced, unbroken fragment of the strandplain. The profiles show horizontal instead of inclined beach foreset layering, suggesting that the gravel underlying the central mounds has been completely reworked by wave action from slumped strandplain gravel. The depth of penetration of radar signals was limited to the top of the water table, that is, about 4–5 m, and thus did not reach the top of the Tertiary deposits.

5 Discussion

5.1 Coseismic deformation

The apparent absence of major seismogenic sources in northern Tierra del Fuego and lands immediately north of the Strait of Magellan, and the relocation of the epicenters for the 1,949 events along the MF fault system allow the inference that this was the more likely source for the large-magnitude seismic events recorded in the study area. This conclusion resolves the doubts posed by Adaros et al. (1999) regarding the dominant seismogenic structure.

The structures affecting the Tertiary substrate at Bustamante and Dungeness Points are interpreted as normal faults. At Bustamante Point, the downstepping of the strandplain is linked indirectly to coseismic faulting of the Tertiary substrate. Faulting must have preceded strandplain accretion over that site. This conclusion is based on two observations. One is that faulting through an overlying strandplain would have truncated some of the curved ridges. The second is that the discordance associated with the fault shows a southwestward concavity roughly parallel to all the ridges and that it dies out inland, which suggests that it developed under the influence of wave action. It is uncertain, however, how much earlier faulting was relative to the discordance. The high-energy wave regime and heavy sand/gravel bedload give rise to strongly abrasive littoral currents. A 10-year control on cliff recession at Dungeness Point indicated an average rate of cliff retreat of 1 m/year. For Bustamante Point, a similar long-term value can be obtained from the 5- to 7-km cliff retreat in, approximately, the past 7 ka. A submerged fault scarp in Tertiary beds subjected to such hydraulic conditions probably would be beveled in a few decades. Mathematical modeling by Trenhaile (2000) showed that intertidal topographic ledges in wave-cut platforms tend to be planed out by wave action.

The collapse structure surveyed at Dungeness Point is associated with a 4 m downthrow of the top of the Tertiary substrate. Seismic shaking could have mobilized saturated strandplain sand and gravel resting on the Tertiary substrate (Fig. 3b), but such movement would not have affected the Tertiary basement significantly. It is inferred from this that collapse occurred in response to deep-seated faulting.

5.2 Recurrence interval

Arguments above suggest that the age of the fault beneath discordance A at Bustamante Point is similar to the age of the ridges that cover it, that is, approximately 3.9 kyr BP

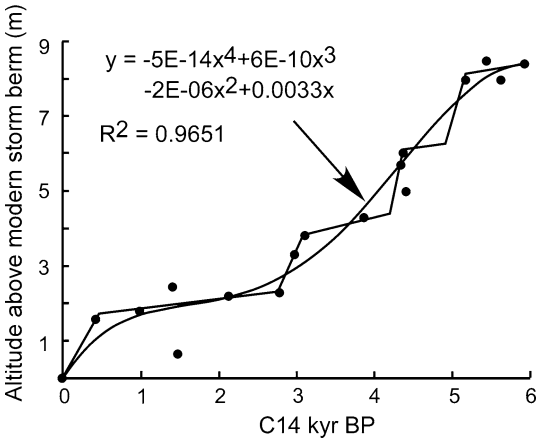

Fig. 5 Elevation versus age of raised Holocene beaches along the Beagle Channel (the Beagle Channel fault in Fig. 2 coincides with the Beagle Channel), with alternative smoothly varying (described by the polynomial with coefficient of regression *R*) and stepwise varying approximations. Data are from Bujalesky (2007)

(Fig. 3a, linear interpolation). Assuming that the other five discordances are underlain by faults and assigning approximate ages to these faults on the basis of overlying ridge ages, the Tertiary substrate at Bustamante Point would have been affected by faulting a minimum of six times, with approximate ages of 0.9, 1.3, 2.4, 3.0, 3.9, and 6.4 kyr BP, giving an average recurrence interval of about 0.9 kyr.

At Dungeness Point, three collapse structures affect the strandplain deposits with ages between, approximately, 7 and 5 kyr BP (Fig. 3b, linear interpolation), with average recurrence rate of 0.7 kyr. These estimates agree with recurrence intervals of damaging earthquakes along the MF fault. Smalley et al. (2003) estimated a recurrence period of 750 years for a $M = 7.8$ earthquake, based on the slip rate of the MF fault, and Waldmann (2008) estimated a recurrence rate of 800–1,000 years for slumps in Lake Fagnano, which he attributed to high-intensity seismic activity on the MF fault system.

A plot of the altitude of raised beaches along the Beagle Channel versus the age of the shelly deposits buried in the fossil berms reflects the continuous uplift of southern Tierra del Fuego island (Fig. 5). The data may be interpreted as reflecting a smoothly varying rate of uplift or an evolution punctuated by coseismic ruptures recurring every 1.2 kyr on average, giving rise to steps 1–2 m in height, an offset that could be accounted for by earthquakes of ca $M = 8$.

Coseismic uplift of marine littoral deposits has been documented, for instance, on the Pacific coast of SW Mexico (Ramírez-Herrera et al. 2004; uplift in excess of 1 m), on the NW coast of Japan (Hiramatsu et al. 2008; 0.44 m uplift), and on the coast of Papua New Guinea (Ota and Chappell 1996; Chappell et al. 1996; average 3 m uplift). In those areas, uplift was distributed over relatively wide coastal expanses. This is in contrast with the results of the present paper that argue for a locally restricted uplift and identify specific causative geologic structures.

5.3 Seismic hazard

The Chile subduction zone south of 52°S, due to the slow plate convergence and the scarce population in its area of influence, southernmost Chile and southwestern sector of Tierra del Fuego island, does not pose a serious seismic hazard. It should be kept in mind for future urban expansion into this region that horizontal peak accelerations of 0.3 g to 0.4 g

have a 10% probability of being exceeded in 50 years (Martin 1990; Algermissen et al. 1992).

The 1949 and 1950 seismic events occurred sequentially from ESE to WNW, suggesting fracture propagation in the sense of relative movement of the South American plate. The epicenters for the 1949 mainshock and foreshock lay about 130 km apart, and those for the 1950 and the 1949 mainshock lay about 230 km apart. The distance between epicenters may reflect segmentation of the main MF fault. Assuming that each epicenter marks the beginning of an asymmetric rupture zone with rupture lengths comparable to epicenter separation, empirical seismic parameter relationships by Wells and Coppersmith (1994) indicate that the estimated rupture lengths could have been associated with magnitude 7.5–8.0 earthquakes, in agreement with earthquake magnitudes recorded for the MF fault system. Coseismic faulting at distances of 300–400 km from the MF fault suggests the occurrence of earthquakes with magnitudes close to 8 along the MF fault in the Holocene. The 1949 and 1950 seismic events originated along the restraining bend of the MF fault, allowing the inference that this segment poses the higher threat to the population of Tierra del Fuego.

The minimum distances between the MF fault and the urban centers of interest to this paper range from less than 1 km (Tolhuin) to almost 100 km (Porvenir). Depending on the chosen attenuation relationship, a magnitude $M = 8$ seismic event would cause a horizontal PGA of approximately 0.3 g (Martin 1990) or 0.11 g (Campbell 1997), at 100 km from the epicenter. The effect may be enhanced by the fact that hypocenters are mainly shallow (Smalley et al. 2003; Buffoni et al. 2009) and also by site amplification of seismic vibrations in areas of soft substrate, particularly in view that all urban centers in Tierra del Fuego have developed, at least in part, on drift and alluvial sediments. Modeling with EERA (Equivalent-linear Earthquake site Response Analyses of Layered Soil Deposits; Bardet et al. 2000) software was carried out on the glacial substrate of Tolhuin urbanization. A 15-m-thick lacustrine clay interval showed potential to amplify seismic waves by a factor of 1.5 (shear modulus and damping for intermediate plasticity clay were stipulated).

6 Conclusions

The epicenters for the four major ($M \geq 7$) instrumentally recorded earthquakes in Tierra del Fuego occurred on the MF fault, or nearby associated faults, indicating that this is the main seismogenic source in Tierra del Fuego. In the absence of a known seismogenic structure closer to the Bustamante and Dungeness Points, it is herein assumed that faults affecting those strandplains resulted from seismic events along the MF fault. A Holocene recurrence interval of about 1,000 years for damaging earthquakes on the MF fault appears well supported by data in this paper and in previous publications. This is in agreement with observations from Costa et al. (2006) showing that the MF fault system was active during the growth of the Bustamante and Dungeness strandplains in the late Holocene. Thus, the MF fault system shows an historic and a prehistoric record of potentially damaging earthquakes that make it the main source of seismic hazard for Tierra del Fuego. Our work provides a framework for progress in estimating the distribution of hazard along the trace of the MF fault. Further geophysical and seismological work is needed for a better characterization of the historical and modern seismic sources.

Acknowledgments This work was funded by the Spanish Ministry of Education and the "Programa de Cooperación con Iberoamérica" of the "Grup de Qualitat de la Generalitat de Catalunya (GRQ94-1048)", Spain, and by the Ministry of Science of Argentina (PICT 32793). Radiocarbon analyses were carried out at the INGEIS-UBA-CONICET laboratory. We acknowledge helpful revisions by reviewers for the Journal.

References

Abascal L del V, González-Bonorino G (2008) Seismic risk associated with the Magallanes-Fagnano continental transform fault, Tierra del Fuego, Southern Argentina. 7th International Symposium on Andean geodynamics (ISAG 2008, Nice), Extended Abstracts, pp 13–16

Adaros RE, Wiens DA, Vera EE, Shore PJ (1999) Seismicity and tectonics of southern Patagonia from a local deployment of seismographs: preliminary results. AEO, 80, Fall Meeting, Suppl, Abstract A52A-05

Algermissen ST, Kausel E, Hanson S, Thenhaus PC (1992) Earthquake hazard in Chile. Revista Geofisica 37:195–218

Annan AP (1992) Ground penetrating radar. Workshop Notes Sensors & Software, Mississauga, p 135

Bardet JP, Ichii K, Lin CH (2000) EERA—a computer program for equivalent-linear earthquake site response analyses of layered soil deposits. Department of Civil Engineering, University of California, California

Barrientos SE (2007) Earthquakes in Chile. In: Moreno T, Gibbons W (eds) The geology of Chile. The Geological Society of London, London, pp 263–289

Buffoni C, Sabbione NC, Connon G, Hormaechea JL (2009) Localización de hipocentros y determinación de su magnitud en Tierra del Fuego y zonas aledañas. Geoacta 34:75–86 Buenos Aires

Bujalesky GG (2007) Coastal geomorphology and evolution of Tierra del Fuego (southern Argentina). Geologica Acta 5:337–362

Campbell KW (1997) Empirical near-source attenuation relationships for horizontal and vertical components of peak ground acceleration, peak ground velocity, and pseudo-absolute acceleration response spectra. Seismological Res Lett 68:154–189

Chappell J, Ota Y, Berryman K (1996) Late quaternary coseismic uplift history of Huon Peninsula, Papua New Guinea. Quat Sci Rev 15:7–22

Christensen N, Mooney W (1995) Seismic velocity structure and composition of the continental crust: a global view. J Geophys Res 100(B7):9761–9788

Costa CH, Smalley R, Schwartz D, Stenner H, Ellis M, Ahumada E, Velasco M-S (2006) Paleoseismic observations of an onshore transform boundary: the Magallanes-Fagnano fault, Tierra del Fuego, Argentina. Rev Asoc Geol Argent 61:647–657

DeMets C, Gordon RG, Argus DF, Stein S (1990) Current plate motions. Geophys J Int 10:425–478

DeMets C, Gordon RG, Argus DF (2010) Geologically current plate motions. Geophys J Int 181:1–80. doi: 10.1111/j.1365-246X.2009.04491.x

Febrer JM, Plasencia MP, Sabbione NC (2001) Local and regional seismicity from Ushuaia broadband station observations (Tierra del Fuego). Terra Antartica 8:35–40

Forsythe DW (1975) Fault plane solutions and tectonics of the South Atlantic and Scotia Sea. J Geophys Res 80:1429–1443

González Bonorino G, Bujalesky G, Colombo F, Ferrero M (1999) Holocene coastal paleoenvironments in Atlantic Patagonia, Argentina. J South Am Earth Sci 12:325–331

Hiramatsu Y, Moriya K, Kamiya T, Kato M, Nishimura T (2008) Fault model of the 2007 Noto Hanto earthquake estimated from coseismic deformation obtained by the distribution of littoral organisms and GPS: implication for neotectonics in the northwestern Noto Peninsula. Earth Planet Space 60:903–913

Jaschek E, Sabbione N, Sierra P (1982) Reubicación de sismos localizados en territorio argentino (1920–1963). Observatorio Astronómico de la Universidad Nacional de La Plata Serie Geofísica, Tomo XI, No 1

Klepeis K (1994) The Magallanes and Deseado fault zones: major segments of the South American-Scotia transform plate boundary in southernmost South America, Tierra del Fuego. J Geophys Res 99:22001–22014

Lawrence JF, Wiens DA (2004) Combined receiver-function and surface wave phase-velocity inversion using a niching genetic algorithm: application to patagonia. Bull Seismol Soc Am 94:977–987

Lodolo E, Menichetti M, Bartole R, Ben-Avraham Z, Tassone A, Lippai H (2003) Magallanes-Fagnano continental transform fault (Tierra del Fuego, southernmost South America). Tectonics 22:15-1-15-26. doi:10.1029/2003TC0901500

Martin A (1990) Hacia una regionalización y cálculo de peligro sísmico en Chile. Dissertation, Universidad de Chile, Santiago

Martinic M (2008) Registro histórico de antecedentes volcánicos y sísmicos en la Patagonia austral y la Tierra del Fuego. Magallania 36:5–18

Menichetti M, Lodolo E, Tassone A (2008) Structural geology of the Fueguian Andes and Magallanes fold-and-thrust belt–Tierra del Fuego island. Geologica Acta 6:19–42

Milne GA, Antony J, Long AJ, Bassett SE (2005) Modelling Holocene relative sea-level observations from the Caribbean and South America. Quat Sci Rev 24:1183–1202

Ota Y, Chappell J (1996) Late quaternary coseismic uplift events on the Huon Peninsula, Papua New Guinea, deduced from coral terrace data. J Geophys Res 101(B3):6071–6082

Palmer D (1980) The generalized reciprocal method of seismic refraction interpretation. Society of Exploration Geophysics, Tulsa, p 104

Pelayo A, Wiens D (1989) Seismotectonics and relative plate motions in the Scotia sea region. J Geophys Res 94:7293–7320

Ramírez-Herrera MT, Kostoglodov V, Urrutia-Fucugauchi J (2004) Holocene-emerged notches and tectonic uplift along the Jalisco coast, Southwest Mexico. Geomorphology 58:291–304

Rubio E, Torné M, Vera E, Díaz A (2000) Crustal structure of the southernmost Chilean margin from seismic and gravity data. Tectonophysics 323:39–60

SEGEMAR (2004) Mapa Geológico de Tierra del Fuego. Servicio Geológico-Minero de Argentina, Buenos Aires Unpublished

SERNAGEOMIN (2003) Mapa Geológico de Chile. Servicio Nacional de Geología y Minería de Chile, Santiago, Publicación Geológica Digital, no 3

Sharma PV (1986) Geophysical methods in geology, 2nd edn. Elsevier, NY

Smalley R Jr, Kendrick E, Bevis M, Dalziel I, Taylor F, Lauría E, Barriga R, Casassa G, Olivero E, Piana E (2003) Geodetic determination of relative plate motion and crustal deformation across the Scotia-South America plate boundary in eastern Tierra del Fuego. Geochem Geophy Geosyst 4:1070. doi: 101029/2002GC000446

Trenhaile AS (2000) Modeling the development of wave-cut shore platforms. Marine Geol 166:163–178

Uribe P, Zamora E (1981) Origen y geomorfología de la Punta Dungeness, Patagonia. Anales Inst de la Patagonia 12:143–158 Punta Arenas

US Army Corps of Engineers (1995) Geophysical exploration for engineering and environmental investigations. Em 1110-1-1802, Washington, DC

Velasco MS, Ellis M, Smalley R Jr (2002) Active faulting in southern Tierra del Fuego. Seismol Res Lett 73:419

Waldmann N (2008) Late Quaternary environmental changes in Lago Fagnano, Tierra del Fuego (54°S): reconstructing sedimentary processes, natural hazards and paleoclimate. Université de Genève, Thèse No 4044, p 149

Wells DL, Coppersmith KJ (1994) New empirical relationships among magnitude, rupture length, rupture width, rupture area, and surface displacement. Bull Seismol Soc Am 84:974–1002